

Superconducting Wigner Vortex Molecule near a Magnetic Disk

M. V. Milošević and F. M. Peeters*
*Departement Natuurkunde, Universiteit Antwerpen (UIA),
 Universiteitsplein 1, B-2610 Antwerpen, Belgium*
 (Dated: February 7, 2020)

Within the non-linear Ginzburg-Landau (GL) theory, we investigate the vortex structure in a superconducting thin film with a ferromagnetic disk on top of it. Antivortices are stabilized in shells around a central core of vortices (or a giant-vortex) with size-magnetization controlled “magic numbers”. An equilibrium vortex phase diagram is constructed. The transition between the different vortex phases occurs through the creation of a vortex-antivortex pair under the magnetic disk edge.

PACS numbers: 74.78.-w, 74.25.Op, 74.25.Dw.

Almost half a century ago, Abrikosov used the Ginzburg-Landau (GL) equations to predict that the magnetic field penetrates a type II superconductor in bundles arranged in a regular lattice, i.e. the vortex lattice [1]. Nowadays, it is well known that the motion of Abrikosov vortices gives rise to dissipation which is the limiting factor for the size of the critical current of a superconductor. The last decade has seen an increased interest in vortex matter in inhomogeneous superconductors, where defects (random and ordered) are used to pin the Abrikosov lattice in order to increase the critical current which is crucial for practical applications. Irradiation by heavy ions allowed to create dense random arrays of columnar defects which increased the critical current density [2]. Thanks to substantial progress in the preparation of magnetic microstructures in combination with superconductors [3], superconductor/ferromagnet hybrid systems became very interesting both theoretically and experimentally. In Ref. [4] Marmoros *et al.* investigated the problem of a magnetic cylinder with out-of-plane magnetization embedded in a superconducting film. They solved the non-linear Ginzburg-Landau equation numerically, with appropriate boundary conditions, and found a correspondence between the value of the magnetization and the vorticity of the giant-vortex states.

More recently, the interest shifted to the pinning behavior of regular arrays of submicron ferromagnetic disks where additional pinning contributions arise due to the magnetic nature of the pinning centers [5, 6]. The most prominent feature of the vortex lattice pinned by a lattice of artificial defects is the existence of matching fields $H_n = n\Phi_0/S$, where Φ_0 is the flux quantum, and S is the area of the primitive cell of the artificial lattice. For matching fields, the number of vortices per unit cell of the artificial lattice becomes an integer number. As expected, such a vortex lattice is pinned much stronger by such artificial defects and the film resistivity exhibits deep minima [5] at those matching fields. These artificial pinning arrays were successfully used to gain insight into the macroscopic commensurability effects, but the origin and microscopic nature of this phenomena have

not yet been fully explained. Moreover, the role of the self-magnetic field of a ferromagnet in the vicinity of the superconductor is not fully understood.

Therefore, in this letter we consider the interaction between a single ferromagnetic disk (FD) and a superconducting thin film (SC), within the non-linear GL theory. The FD lies on top of the superconductor (xy plane) and it is magnetized in the positive z -direction. To avoid the proximity effect and exchange of electrons between FD and SC we separate them by a thin layer of insulating oxide, as is usually the case in experimental conditions. Moreover, we consider the magnetic disk to be made of a hard magnet whose uniform magnetic moment and internal currents are not affected by nearby circulating supercurrents. The ferromagnetic disk is the only source of magnetic field and we study in detail how the system is perturbed in the neighborhood of the disk. The creation of vortices due to this field, as well as their behavior strongly influence the pinning of additional external flux lines. Furthermore, we find new ordered vortex/antivortex structures.

For thin superconductors ($d < \xi, \lambda$) it is allowed to average the GL equations over the film thickness and write them as

$$\left(-i\vec{\nabla}_{2D} - \vec{A}\right)^2 \Psi = \Psi \left(1 - |\Psi|^2\right), \quad (1)$$

$$-\Delta_{3D} \vec{A} = \frac{d}{\kappa^2} \delta(z) \vec{j}_{2D}, \quad (2)$$

where

$$\vec{j}_{2D} = \frac{1}{2i} \left(\Psi^* \vec{\nabla}_{2D} \Psi - \Psi \vec{\nabla}_{2D} \Psi^*\right) - |\Psi|^2 \vec{A}, \quad (3)$$

is the density of superconducting current and \vec{A} is the total vector potential from the FD and supercurrents, with boundary condition $\vec{A} = 0$ far away from the FD. Here the distance is measured in units of the coherence length ξ , the vector potential in $c\hbar/2e\xi$, and the magnetic field in $H_{c2} = c\hbar/2e\xi^2 = \kappa\sqrt{2}H_c$. The indices $2D$, $3D$ refer to two- and three-dimensional operators,

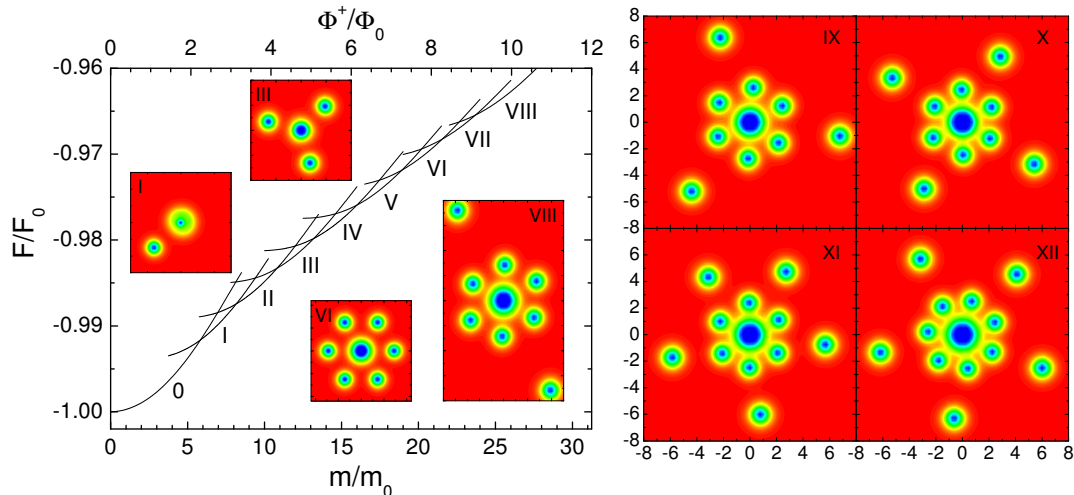


FIG. 1: The Gibbs free energy as a function of the magnetic moment of the disk with radius $R_d/\xi = 1$ placed on top of the superconductor. Top axis shows the flux captured by the superconductor in the positive stray field area of the magnetic disk. Insets and figures on the right are the contourplots of the Cooper pair density (red/blue): high(low) density) for a few ground state vortex configurations. A giant-vortex is surrounded by antivortices, and the total vorticity equals zero. Only 1/16 of the total simulation area is shown.

respectively. To solve the system of Eqs. (1-2), we apply a finite-difference representation of the order parameter and the vector potential on a uniform Cartesian space grid (x,y) , with typically 512 grid points along the width of the rectangular simulation region $L_{x(y)}$, and use the link variable approach [7], and an iteration procedure based on the Gauss-Seidel technique to find Ψ . The vector potential is then obtained with the fast Fourier transform technique. The first GL equation is solved with an iteration procedure [8]. The dimensionless Gibbs free energy is calculated as $F = V^{-1} \int (2(\vec{A} - \vec{A}_0) \cdot \vec{j}_{2D} - |\Psi|^4) d\vec{r}$, where integration is performed over the primitive cell volume V , and \vec{A}_0 is the vector potential of the magnetic disk. The periodic boundary conditions for \vec{A} and Ψ have the form [9]

$$\vec{A}(\vec{\rho} + \vec{b}_i) = \vec{A}(\vec{\rho}) + \vec{\nabla} \eta_i(\vec{\rho}), \quad (4)$$

$$\Psi(\vec{\rho} + \vec{b}_i) = \Psi \exp(2\pi i \eta_i(\vec{\rho}) / \Phi_0), \quad (5)$$

where \vec{b}_i , $i = x, y$ are the lattice vectors, and η_i is the gauge potential which cannot be chosen freely but must preserve the single valuedness of \vec{A} and Ψ . These boundary conditions mean that \vec{A} , Ψ are invariant under lattice translations combined with specific gauge transformations [9]. Other quantities, such as the magnetic field, the current and the order parameter density are periodic. We choose $\eta_x = A_{0x}$, $\eta_y = A_{0y}$, with the simulation region typically hundred times larger than the magnetic disk, i.e. $L_x \gg R_d$, which implies the quantization of the flux, namely total flux through the superconductor equals zero. These boundary conditions result in a periodic repetition of not only the superconductor but the magnetic disk lattice as well. However, due to the large simulation region, these disks are far from each other and we are allowed to treat this problem as a single disk on top of an infinite superconductor.

To find the different vortex configurations, which include the metastable states, we search for the steady-state solutions of Eqs. (1) and (2) starting from different randomly generated initial configurations. Then we increase/decrease slowly the magnetic moment of the magnetic disk m and recalculate each time the exact vortex structure. We do this for each vortex configuration in a magnetic moment (m) range where the number of vortices remains constant. By comparing the Gibbs free energies of the different vortex configurations we obtain the ground state. The results are shown in Fig. 1 for the magnetic disk with radius $R_d/\xi = 1$ and thickness $d_d/\xi = 0.5$, on top of the superconductor with thickness $d/\xi = 0.5$. The magnetic moment is expressed in units of $m_0 = \hbar \xi / 2e = H_{c2} \xi^3$. Demagnetization effects are taken into account in this calculation and the Ginzburg-Landau parameter κ was chosen to be 1, which approximately corresponds to the experimental values found for Pb, Nb, or Al films. The values for d , d_d and κ mentioned above will be used throughout this paper.

From Fig. 1, we notice that with increasing magnetization of the ferromagnetic disk, the ground state goes through different vortex states denoted by successive Roman numerals. In the case of a finite extend of the superconducting film, i.e. thin mesoscopic disks, with a magnetic disk on top [10], the Roman numerals corresponded to the vorticity of the ground state. However, in that case, the total flux penetrating the finite size superconductor was positive, and therefore, the states with positive vorticity dominated the free energy diagram. In the present case, the magnetic disk is on top of an infinite SC film, consequently all flux is captured by the superconductor, and the total penetrating flux equals zero. Due to phase conservation, vortices cannot appear individually, but only as vortex-antivortex pairs. The vortex

is located under the disk, and the antivortex just outside the positive field region. In Fig. 1, each new vortex state corresponds to the appearance of a new vortex-antivortex pair. Because the magnetic disk is relatively small, vortices are strongly confined by the positive magnetic field under the disk, which leads to a giant-vortex as the energetically favorable state, while antivortices are symmetrically arranged on a ring around the central vortex (see Fig. 1). The Cooper pair density contourplots in Fig. 1 show the states in question for the particular value of the magnetic moment of the disk when they become the ground state, namely at the crossing points of the free energy curves. With increasing magnetization of the disk and fixed vortex state, the antivortices move further away from the magnetic disk. The configurations shown in Fig. 1 are the result not only of the magnetic field of the ferromagnetic disk, but also of the interaction between the vortices. While the giant-vortex strongly attracts the antivortices, the antivortices repel each other. One therefore expects that the vortex configurations strongly depend on the size of the magnetic disk, since it determines the distance between the giant-vortex and the antivortices, and the circumference of the circle the antivortices are located on.

Because the vortex configuration is determined by the balance between the giant vortex-antivortex attraction and the repulsion between antivortices, it is clear that the number of antivortices on a ring around the giant-vortex cannot increase monotonously. Actually, the formation of a second, or of even more rings is possible with increasing m (see Fig. 1, for the states with $N = 9 - 12$, where N denotes the number of antivortices). A second ring is formed when the number of antivortices reaches a saturation value n_s (or “magic number”), in our case this occurs for $n_s = 6$. This, however, does not mean that the number of vortices in the first ring remains constant with increasing magnetization. For example for $N = 12$ it turns out that one more antivortex fits in the first ring.

Since the antivortices are arranged around the positive magnetic field region, the saturation number n_s should depend on the size of the magnetic disk. Furthermore, for larger disks the wider area of the positive field region under the disk could allow the giant-vortex under the disk to split into individual vortices. Therefore, we investigated the influence of the disk size on the vortex structure of the superconducting film. We enlarged the magnetic disk from $R_d/\xi = 0.5$ to 5 keeping the thickness d_d and the parameters of the SC fixed. In doing so, we obtain the equilibrium vortex phase diagram, shown in Fig. 2. Solid lines correspond to transitions between the successive N states, and the thick dashed lines give the number of antivortices needed for the formation of an additional ring of antivortices. In the white (shaded) region the giant- (multi-) vortex state is found under the magnetic disk.

Notice that with enlarging the magnetic disk the num-

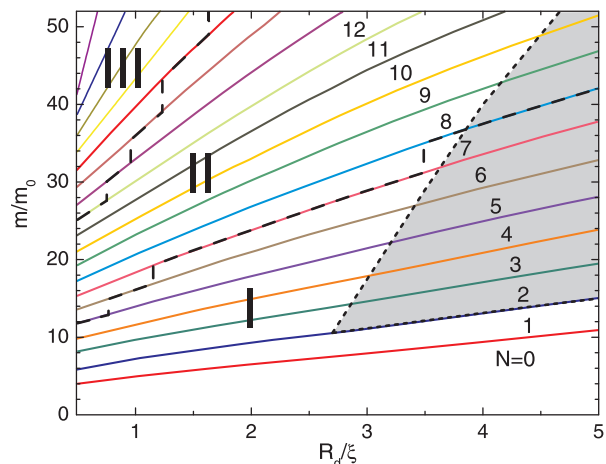


FIG. 2: Phase diagram: the relation between the radius of the disk, its magnetic moment, the number of antivortices (N), the number of antivortex rings (Roman numbers) and the vortex state under the magnetic disk (shaded area: multivortex state).

ber of antivortices needed before a new ring is formed increases, as expected. But, on the other hand a larger magnetic moment is needed for the appearance of a new vortex-antivortex pair in the ground state. However, the volume of the disk also increases, which diminishes the effects of the magnetic moment increase. Therefore, we calculated the flux Φ^+ through the SC, due to the positive part of the stray field in the $z = 0$ plane, namely in the center of the superconductor and up to the radius $R_0 \simeq R_d$ where the magnetic field changes its polarity. The top axis in Fig. 1 shows the value of this flux. Such a calculation tells us that if we keep the magnetic moment constant and increase the radius (volume) of the disk, the flux Φ^+ decreases, making the positive (and negative) flux through the SC approximately constant along the transition line between the successive states in Fig. 2. Obviously, a larger flux is needed to create the first vortex-antivortex pair, i.e. $\Delta\Phi^+/\Phi_0 = 2.112$, due to the high stability of the Meissner state and the asymmetry of the $N = 1$ state (see inset of Fig. 1). Further increase of the flux Φ^+ decreases $\Delta\Phi^+$ and for larger N it approaches the value $\Delta\Phi^+/\Phi_0 = 1.073$. Notice that the flux Φ^+ is not exactly quantized in units of Φ_0 which is a mesoscopic effect. The quantization condition $\Phi = \oint_C \vec{A} \cdot d\vec{l} = L\Phi_0$ cannot be used because it is not possible to construct a contour C around the positive stray field region where the current is zero.

With increasing radius of the disk, the giant-vortex splits into individual vortices, as shown in Fig. 3(a). Figure 3(b) shows the phase of the superconducting order parameter, from which the location of the vortices and antivortices can be easily deduced. With increasing magnetic field, these vortices move closer together, resulting ultimately in the formation of a giant-vortex. Figs. 3(c,d) show the current distribution in the SC: the supercurrents around each vortex and antivortex flow in

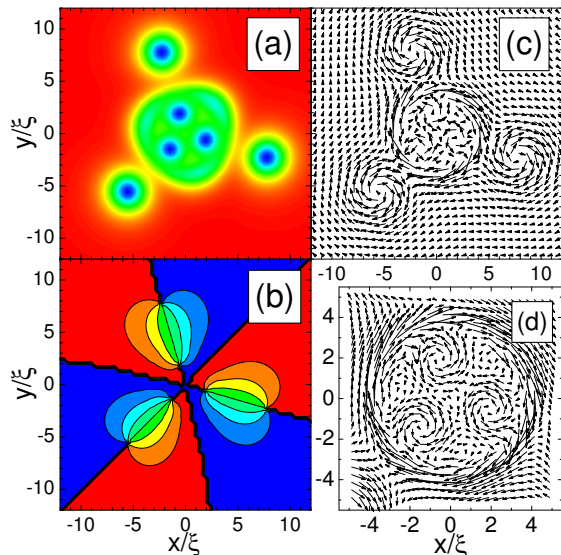


FIG. 3: Splitting of the giant-vortex under the disk into a multivortex: a) Cooper pair density, b) superconducting phase contourplot (zero - blue, 2π - red), for $N = 3$, $R_d/\xi = 4.0$, and $m/m_0 = 18.5$. (c) is a vectorplot of the corresponding supercurrents and (d) is an enlargement of the central area.

opposite directions, which are determined by the direction of the change of the phase of the order parameter. However, the current around the central vortices (i.e. at the edge of the magnetic disk) has the same direction as the one around the antivortices, although the phase change implies otherwise. The reason is that the direction of this supercurrent is governed by the vector potential of the magnetic field of the ferromagnetic disk which is maximal near the edge of the disk. The value of the total current will be maximal in the same region. This is also the reason why with increasing magnetic moment of the FD new vortices nucleate exactly under the edge of the disk, i.e. when the maximal current reaches the value of the GL current.

To analyze the generation of new vortices, we start from one specific initial condition, for example, the ground state configuration for $N = 3$. Then we increase slowly the magnetic moment of the magnetic disk m and recalculate the vortex structure within 10^5 iteration steps for each value of m . This way we can find the magnetic moment for which the initial state changes from $N = 3$ to the $N = 4$ configuration and we observe the nucleation of a vortex-antivortex pair by plotting the intermediate results during the different iteration steps. The result for the III \rightarrow IV transition is shown in Fig. 4. The Cooper pair density plot Fig. 4(a) shows only a distorted central vortex, but the superconducting phase plot (b) reveals the real vortex structure. Namely, in addition to the configuration similar to the state III, one can notice a vortex-antivortex pair nucleating under the edge of the dot. Further iterations in our calculation show that the vortex from this pair will move towards the central giant-vortex and the antivortex moves to the periphery,

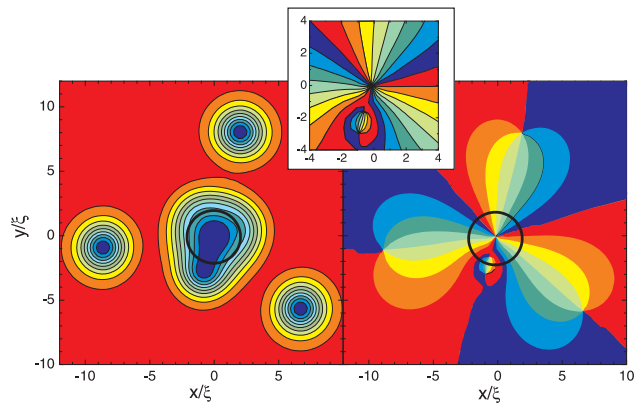


FIG. 4: Generation of the vortex-antivortex pair with increasing magnetic moment of the disk: a) Cooper pair density, and b) superconducting phase contourplot, for $N = 3(4)$ and $R_d/\xi = 2.0$. The thick ring shows the edge of the FD. The upper inset is an enlargement of the phase of the central area which more clearly shows the vortex-antivortex pair.

causing the rearrangement of the shell of antivortices into the configuration IV.

The predicted new vortex configurations can be observed experimentally by using e.g. scanning probe techniques like Hall and Magnetic Force Microscopy. Furthermore, these vortex structures will influence the pinning properties and the superconducting phase diagram [11].

The authors acknowledge D. Vodolazov for fruitful discussions. This work was supported by the Flemish Science Foundation (FWO-VI), IUAP, GOA, and the ESF programme on “Vortex matter”.

* Electronic address: peeters@uia.ua.ac.be

- [1] A.A. Abrikosov, Zh. Eksp. Teor. Fiz. **32**, 1442 (1957).
- [2] L. Civale, A.D. Marwick, T.K. Worthington, M.A. Kirk, J.R. Thompson, L. Krusin-Elbaum, Y. Sun, J.R. Clem, and F. Holtzberg, Phys. Rev. Lett. **67**, 648 (1991).
- [3] J.I. Martin, M. Velez, J. Nogues, and I.K. Schuller, Phys. Rev. Lett. **79**, 1929 (1997).
- [4] I.K. Marmoros, A. Matulis, and F.M. Peeters, Phys. Rev. B **53**, 2677 (1996).
- [5] J.I. Martin, M. Velez, A. Hoffmann, I.K. Schuller, and J.L. Vicent, Phys. Rev. Lett. **83**, 1022 (1999).
- [6] M.J. Van Bael, K. Temst, V.V. Moshchalkov, and Y. Bruynseraede, Phys. Rev. B **59**, 14674 (1999).
- [7] R. Kato, Y. Enomoto, and S. Maekawa, Phys. Rev. B **47**, 8016 (1993).
- [8] V.A. Schweigert, F.M. Peeters, and P.S. Deo, Phys. Rev. Lett. **81**, 2783 (1998).
- [9] M.M. Doria, J.E. Gubernatis, and D. Rainer, Phys. Rev. B **39**, 9573 (1989).
- [10] M. V. Milošević, S. V. Yampolskii, and F. M. Peeters, Phys. Rev. B **66**, 024515 (2002).
- [11] M. Lange, M.J. Van Bael, Y. Bruynseraede, and V.V. Moshchalkov, cond-mat/0209101.